

MODELLING OF HYSTERETIC AND ANISOTROPIC MAGNETIC FIELD PROBLEMS

Y. Saito, H. Saotome, S. Hayano and T. Yamamura

**Abstract** - Previously, a modelling of magnetodynamic fields taking into account dynamic hysteresis loops was proposed for predicting three-dimensional magnetodynamic fields in electromagnetic devices. This method is now generalized to take into account the anisotropic property due to the lamination of iron sheets, and improved with respect to the time discretization method.

This improved modelling of hysteretic and anisotropic magnetic fields is applied to a simple toroidal transformer, whose various characteristics are calculated and compared with experimental measurements.

INTRODUCTION

A recent paper had proposed a modelling of magnetodynamic fields taking into account dynamic hysteresis loops for predicting three-dimensional magnetodynamic fields in electromagnetic devices [1]. Also, the success of the Saito equation in the modelling of hysteretic magnetodynamic fields spurred Saito, Saotome and Yamamura to construct the lumped circuit model for nonlinear inductor exhibiting dynamic hysteresis loops [2]. In this paper, the Saito equation in the modeling of hysteretic magnetodynamic fields is generalized to take into account the anisotropic property due to the lamination of iron sheets, and improved with respect to the time discretization method. The anisotropic property due to the lamination of iron sheets is introduced in terms of the space factor of iron, and the time discretization method is improved in cooperation with the magnetic circuit connection. Thus, this improved modelling of hysteretic and anisotropic fields is now applied to a simple toroidal transformer, whose various characteristics are calculated and compared with experimental measurements.

THEORY OF MAGNETIC CIRCUITS

The Saito equation in the modelling of hysteretic magnetodynamic fields is given by

$$H = \left(\frac{1}{\mu}\right)B + \left(\frac{1}{s}\right)\frac{dB}{dt} \tag{1}$$

where  $H, B, \mu$  and  $s$  are the magnetic field intensity, flux density, permeability and hysteresis coefficient, respectively. For further details of (1), you may refer to [1].

Two-Dimensional Hysteretic Magnetic Fields

By considering (1) and the region bounded by the contour  $\overline{abcd\bar{a}}$  in Fig. 1(a), it is possible to write the following relation:

$$\int_{\overline{abcd\bar{a}}} H dl = \int_{\overline{abcd\bar{a}}} \left[ \left(\frac{1}{\mu}\right)B + \left(\frac{1}{s}\right)\frac{dB}{dt} \right] dl, \tag{2}$$

where  $dl$  denotes the infinitesimally small distance along with the contour  $\overline{abcd\bar{a}}$ . The left-hand term in (2) is related to the current density  $J_1$  as

$$\int_{\overline{abcd\bar{a}}} H dl = A_{\overline{abcd\bar{a}}} \int J_1 n da = i_1, \tag{3}$$

where  $da$  is the infinitesimally small area,  $A_{\overline{abcd\bar{a}}}$  is the surface area bounded by the contour  $\overline{abcd\bar{a}}$  and  $n$  is the unit normal vector on the infinitesimally small area  $da$ . In (3), it is assumed that the current  $i_1$  is

The authors are with College of Engineering, Hosei University, 3-7-2 Kajinocho Koganei, Tokyo 184, Japan.

not uniformly distributed on the surface  $A_{\overline{abcd\bar{a}}}$ , but concentrated on the conductor with infinitesimally small cross-sectional area located at the mesh point of surface  $A_{\overline{abcd\bar{a}}}$ . Similarly, it is assumed that the currents in the other regions in Fig. 1(a) are concentrated on the conductors with infinitesimally small cross-sectional area located at each of their mesh points. Due to the nonlinear magnetization characteristic of iron, it is assumed that both the permeability  $\mu$  and hysteresis coefficient  $s$  in (2) are position dependent. Furthermore, it is assumed that the region which encloses each of the mesh points in Fig. 1(a) may have a constant permeability and hysteresis coefficient.

The magnetic field intensity  $H$  and flux density  $B$  may take different values with respect to position, but it is possible to assume that the magnetic flux which takes a path between the mesh points may take a constant value. With these assumptions, the magnetic fields in Fig. 1(a) may be calculated for a modified form in the regions as shown in Fig. 1(b) without any appreciable error. Thereby, the current  $i_1$  in (3) can be expressed in terms of the flux  $\phi_1$ , impressed voltage  $e_1$  and electric resistance  $r_1$ . Also, the right-hand term in (2) can be expressed by the magnetic resistance  $R_{1k}$  and hysteresis coefficient  $S_{1k}$ . Accordingly, (2) may be rewritten by

$$\left(\frac{1}{r_1}\right)[e_1 - (d/dt)\phi_1] = \sum_{k=2}^5 [R_{1k} + S_{1k} (d/dt)] [\phi_1 - \phi_k]. \tag{4}$$

(4) means that the magnetic circuits of the regions in Fig. 1(b) are formally drawn as Fig. 1(c). The magnetic resistance calculations with various geometrical shapes are described in [3]. By considering the right-hand terms in (2) and (4), it is found that the parameter which depends on the geometrical shape is common to both  $R_{1k}$  and  $S_{1k}$ . Therefore, the hysteresis parameters for various geometrical shapes are calculated in much the same way as the magnetic resistance. Also, the electric resistance  $r_1$  in (4) is calculated in much the same way as the magnetic resistance, because the definition of electric resistance with respect to the geo-

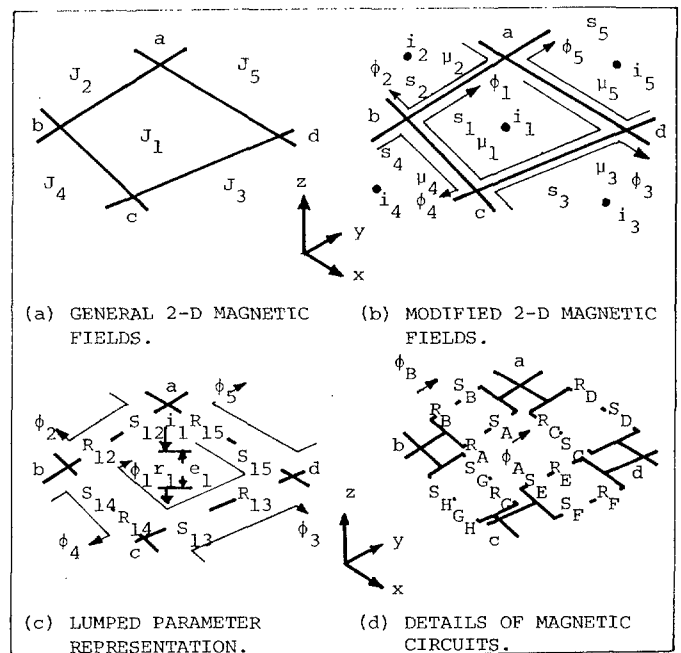


Fig. 1. Two-dimensional hysteretic magnetic fields.

metrical shape is similar to the definition of magnetic resistance [4].

#### Boundary Conditions

At the interfaces of different materials, the tangential component of magnetic field intensity as well as the normal component of flux density must be continuous.

When we assume that the magnetic circuits of Fig. 1(b) may be drawn as Fig. 1(d), then it is obvious that the boundary condition related to the tangential component of magnetic field intensity is always satisfied. The other boundary condition related to the normal component of flux density is taken into account in the calculations of magnetic resistance and hysteresis parameter [3].

#### Discretization in Time Dependent Terms

The magnetic circuit equation between nodes a and b in Fig. 1(d) is

$$f_{ab} = R_A \phi_A + S_A (d\phi_A/dt) = R_B \phi_B + S_B (d\phi_B/dt), \quad (5)$$

where  $f_{ab}$  denotes the magnetomotive force between nodes a and b in Fig. 1(d); the magnetic resistances  $R_A, R_B$ , hysteresis parameters  $S_A, S_B$  and fluxes  $\phi_A, \phi_B$  are shown in Fig. 1(d). By means of a finite difference approach, (5) is discretized in time by

$$\begin{aligned} f_{ab}(t+\alpha\Delta t) &= z_A^p(t+\alpha\Delta t)\phi_A(t+\Delta t) - z_A^n(t+\alpha\Delta t)\phi_A(t) \\ &= z_B^p(t+\alpha\Delta t)\phi_B(t+\Delta t) - z_B^n(t+\alpha\Delta t)\phi_B(t), \end{aligned} \quad (6)$$

where  $\Delta t$  denotes the stepwidth in time  $t$ ; the magnetomotive force  $f_{ab}(t+\alpha\Delta t)$ , and magnetic resistances  $z_A^p(t+\alpha\Delta t), z_A^n(t+\alpha\Delta t), z_B^p(t+\alpha\Delta t), z_B^n(t+\alpha\Delta t)$  are

$$\begin{aligned} f_{ab}(t+\alpha\Delta t) &= \alpha f_{ab}(t+\Delta t) + (1-\alpha)f_{ab}(t), \\ z_A^p(t+\alpha\Delta t) &= (1/\Delta t) [S_A(t+\alpha\Delta t) + \alpha\Delta t R_A(t+\alpha\Delta t)], \\ z_A^n(t+\alpha\Delta t) &= (1/\Delta t) [S_A(t+\alpha\Delta t) - (1-\alpha)\Delta t R_A(t+\alpha\Delta t)], \\ z_B^p(t+\alpha\Delta t) &= (1/\Delta t) [S_B(t+\alpha\Delta t) + \alpha\Delta t R_B(t+\alpha\Delta t)], \\ z_B^n(t+\alpha\Delta t) &= (1/\Delta t) [S_B(t+\alpha\Delta t) - (1-\alpha)\Delta t R_B(t+\alpha\Delta t)], \\ R_A(t+\alpha\Delta t) &= \alpha R_A(t+\Delta t) + (1-\alpha)R_A(t), \\ R_B(t+\alpha\Delta t) &= \alpha R_B(t+\Delta t) + (1-\alpha)R_B(t), \\ S_A(t+\alpha\Delta t) &= \alpha S_A(t+\Delta t) + (1-\alpha)S_A(t), \\ S_B(t+\alpha\Delta t) &= \alpha S_B(t+\Delta t) + (1-\alpha)S_B(t), \end{aligned} \quad (7)$$

The parameter  $\alpha$  in (6), (7) may be chosen arbitrary e.g.  $\alpha=0, \alpha=1$  yield forward and backward differences, respectively. In (6), it is assumed that the terms  $z_A^p(t+\alpha\Delta t)\phi_A(t+\Delta t)$  and  $z_A^n(t+\alpha\Delta t)\phi_A(t)$  correspond to  $z_B^p(t+\alpha\Delta t)\phi_B(t+\Delta t)$  and  $z_B^n(t+\alpha\Delta t)\phi_B(t)$ , respectively. Thereby, (6) can be expressed in terms of the loop fluxes  $\phi_1(t+\Delta t), \phi_1(t), \phi_2(t+\Delta t), \phi_2(t)$  in Fig. 1(c) as

$$\begin{aligned} f_{ab}(t+\alpha\Delta t) &= z_{12}^p(t+\alpha\Delta t) [\phi_1(t+\Delta t) - \phi_2(t+\Delta t)] \\ &\quad - z_{12}^n(t+\alpha\Delta t) [\phi_1(t) - \phi_2(t)], \end{aligned} \quad (8)$$

where

$$\begin{aligned} z_{12}^p(t+\alpha\Delta t) &= \frac{z_A^p(t+\alpha\Delta t)z_B^p(t+\alpha\Delta t)}{z_A^p(t+\alpha\Delta t) + z_B^p(t+\alpha\Delta t)}, \\ z_{12}^n(t+\alpha\Delta t) &= \frac{z_A^n(t+\alpha\Delta t)z_B^n(t+\alpha\Delta t)}{z_A^n(t+\alpha\Delta t) + z_B^n(t+\alpha\Delta t)}. \end{aligned} \quad (9)$$

The other magnetic circuit equations between the nodes in Fig. 1(d) can be obtained in much the same way as (8), and combining these magnetic circuit equations, the right-hand term in (4) is represented in time discretized form as

$$\sum_{k=2}^5 [R_{1k} + S_{1k} (d/dt)] [\phi_1 - \phi_k] = \sum_{k=2}^5 [z_{1k}^p(t+\alpha\Delta t) \{\phi_1(t+\Delta t) - \phi_k(t+\Delta t)\} - z_{1k}^n(t+\alpha\Delta t) \{\phi_1(t) - \phi_k(t)\}], \quad (10)$$

where  $z_{1k}^p(t+\alpha\Delta t), z_{1k}^n(t+\alpha\Delta t)$  ( $k=3,4,5$ ) are the magnetic impedances between the nodes b, c, d, a in Fig. 1(d).

By means of a finite difference method, the left-hand term in (4) is replaced by the following equation:

$$\begin{aligned} (1/r_1) [e_1 - (d/dt)\phi_1] &= (1/r_1) [\alpha e_1(t+\Delta t) + (1-\alpha)e_1(t) \\ &\quad - (1/\Delta t) \{\phi_1(t+\Delta t) - \phi_1(t)\}]. \end{aligned} \quad (11)$$

Substituting (10), (11) into (4) and rearranging, the magnetic circuit equation discretized in time is given by

$$\begin{aligned} f_1(t+\alpha\Delta t) + \left[ \frac{1}{r_1 \Delta t} + \sum_{k=2}^5 z_{1k}(t+\alpha\Delta t) \right] \phi_1(t) \\ - \sum_{k=2}^5 z_{1k}^n(t+\alpha\Delta t) \phi_k(t) = \left[ \frac{1}{r_1 \Delta t} + \sum_{k=2}^5 z_{1k}^p(t+\alpha\Delta t) \right] \phi_1(t+\Delta t) - \sum_{k=2}^5 z_{1k}^p(t+\alpha\Delta t) \phi_k(t+\Delta t), \end{aligned} \quad (12)$$

where the externally impressed magnetomotive force  $f_1(t+\alpha\Delta t)$  is

$$f_1(t+\alpha\Delta t) = (1/r_1) [\alpha e_1(t+\Delta t) + (1-\alpha)e_1(t)]. \quad (13)$$

#### Anisotropic Magnetization

In order to suppress the eddy currents flowing through the iron core, electromagnetic devices are always constructed by the lamination using insulated iron sheets. This makes the magnetization characteristic of the iron core anisotropic in direction. For an example, consider the magnetization characteristic of the iron core shown in Fig. 2. It is obvious that the permeability and hysteresis coefficient of this iron core may take different values with respect to direction. Generally, the space occupied by the insulation materials in the iron core is very small, and may be regarded as air gap. Moreover the permeability of air has a very small value compared with that of iron, and the hysteresis coefficient of air takes an infinitely large value. Therefore, it is a rational assumption that all of the flux in the direction of x-axis in Fig. 2 will flow through the path containing iron. This means that the permeability  $\mu_x$  and hysteresis coefficient  $s_x$  in Fig. 2 are given by

$$\begin{vmatrix} \mu_x \\ s_x \end{vmatrix} = \begin{vmatrix} \gamma & 0 \\ 0 & \gamma \end{vmatrix} \begin{vmatrix} x \\ x \end{vmatrix} \begin{vmatrix} \mu \\ s \end{vmatrix}, \quad (14)$$

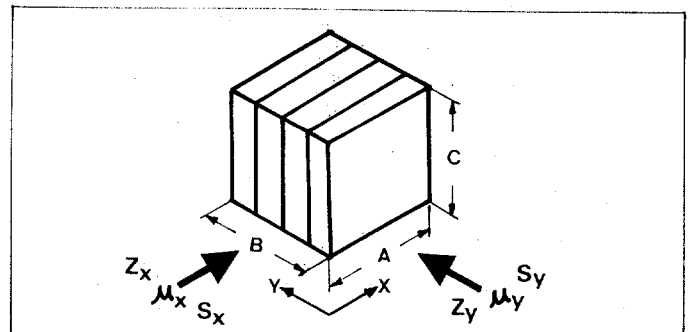


Fig. 2. An example of laminated core.

where  $\gamma$  is the space factor of iron viz.,  $\gamma = \frac{\text{VOLUME OF IRON}}{\text{TOTAL VOLUME OF IRON CORE}}$ . On the contrary, all of the flux in the direction of y-axis must flow through the path containing iron as well as air. Therefore, the permeability  $\mu_y$  and hysteresis coefficient  $s_y$  in Fig. 2 are given by

$$\begin{vmatrix} \mu_y \\ s_y \end{vmatrix} = \begin{vmatrix} \frac{1}{\gamma + (1-\gamma)(\mu/\mu_0)} & 0 \\ 0 & (1/\gamma) \end{vmatrix} \times \begin{vmatrix} \mu \\ s \end{vmatrix}, \quad (15)$$

where  $\mu_0$  is the permeability of air. The relationships of (14), (15) have been derived for a simple rectangular prism element. Nevertheless, the results of (14), (15) are valid for the other shapes of element.

Three-Dimensional Hysteretic Magnetic Fields

Most electromagnetic devices consist of conducting wires around an iron core; in order to minimize the magnetic field energy stored in the iron core, the eddy currents in the iron core flow in a direction opposite to the exciting current. The magnetic flux which passes through the path parallel to the current carrying coil can be neglected, therefore, it is preferable to consider the solid element as shown in Fig. 3(a).

This three-dimensional element can be represented by the two-dimensional coordinate, which consists of the radial and tangential directions. For simplicity, it is preferable to consider an example. One of the simplest examples of electromagnetic devices is the toroidal transformer as shown in Fig. 3(b). This is divided into  $M_R$  parts in the radial direction and  $M_T$  parts in the tangential direction, taking into account the region containing air. Thereby, the magnetic field calculation of the toroidal transformer is reduced to evaluating the  $M$  ( $=M_R \times M_T$ ) loop fluxes. Moreover, it is assumed that each of the coils covers a distinct solid element which is similar in shape to the solid element shown in Fig. 3(a). The system of magnetic circuit equations is best expressed in matrix notation involving the externally impressed magnetomotive force vector  $F[t+\alpha\Delta t]$ , initial flux vector  $\Phi[t]$ , flux vector  $\Phi[t+\Delta t]$ , electric conductance matrix  $G$ , initial magnetic impedance matrix  $Z^N[t+\alpha\Delta t]$  and magnetic impedance matrix  $Z^P[t+\alpha\Delta t]$ , that is

$$F[t+\alpha\Delta t] + \{G + Z^N[t+\alpha\Delta t]\}\Phi[t] = \{G + Z^P[t+\alpha\Delta t]\}\Phi[t+\Delta t]. \quad (16)$$

When we compared the magnetic circuits in Fig. 3(b) with (16), then it is found that the loop flux  $\Phi_{M+1}$  [shown in dotted line in Fig. 3(b)] must be taken into account in the calculation of fluxes to satisfy the condition of minimum number of network equations. Since the loop flux  $\Phi_{M+1}$  in Fig. 3(b) is physically flowing in a tangential direction at the center of figure, we can find the following relationships:

$$\Phi[t] = C^T \Phi_c[t], \quad \Phi[t+\Delta t] = C^T \Phi_c[t+\Delta t], \quad (17)$$

where subscript c refers to the three-dimensional quantities, superscript T denotes the transpose of matrix, and  $C^T$  is the flux connection matrix which is a rectangular matrix with M rows and M+1 columns:

$$C^T = \begin{vmatrix} 1 & 0 & 0 & \dots & -1 \\ 0 & 1 & 0 & \dots & -1 \\ \dots & \dots & \dots & \dots & \dots \\ 0 & 0 & 0 & \dots & -1 \end{vmatrix}. \quad (18)$$

Since the magnetomotive force due to the initial flux vector  $\Phi[t]$  may be considered as one of the input vectors, the system of three-dimensional magnetic circuit equations is given by

$$\begin{aligned} F_c[t+\alpha\Delta t] + \{G_c + Z_c^N[t+\alpha\Delta t]\}\Phi_c[t] \\ = \{G_c + Z_c^P[t+\alpha\Delta t]\}\Phi_c[t+\Delta t], \end{aligned} \quad (19)$$

where

$$\begin{aligned} F_c[t+\alpha\Delta t] &= CF[t+\alpha\Delta t], & G_c &= CGC^T, \\ Z_c^N[t+\alpha\Delta t] &= CZ^N[t+\alpha\Delta t]C^T, & Z_c^P[t+\alpha\Delta t] &= CZ^P[t+\alpha\Delta t]C^T. \end{aligned} \quad (20)$$

COMPARISON WITH EXPERIMENT

The flux vector  $\Phi_c[t+\Delta t]$  in (19) is calculated by iteration, using a relaxation parameter [3]. Fig. 4 shows the magnetization curves of iron. Various constants used in the calculations of the toroidal transformer are listed in Table 1. Because of the simplicity of the calculations and usefulness for examining the eddy currents (namely load current may be considered as one of the eddy currents), we selected the pure resistive loads. The parameters  $\alpha$  and  $\Delta t$  in (19) were respectively determined as  $\alpha=0.5$  and  $\Delta t=0.25$  (msec) by the numerical tests when the convergence and accuracy of the solutions were taken into account. The toroidal transformer in Fig. 3(b) has four secondary

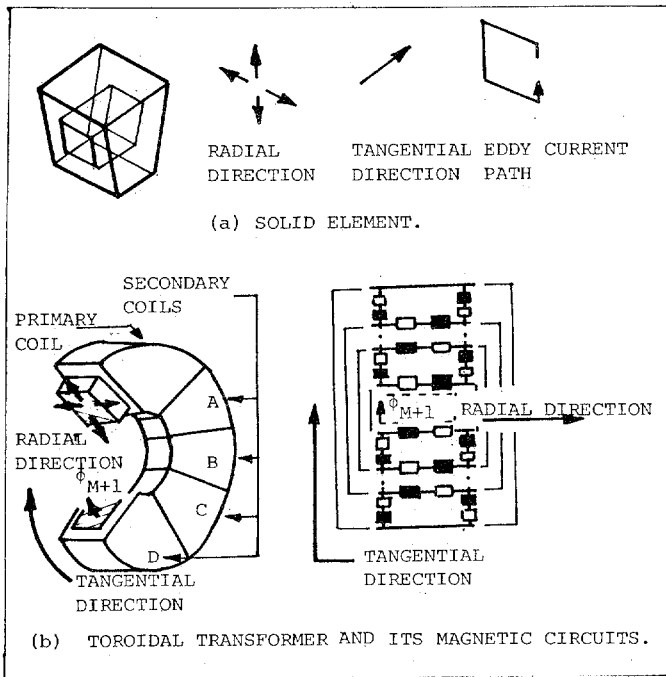


Fig. 3. Solid element and toroidal transformer.

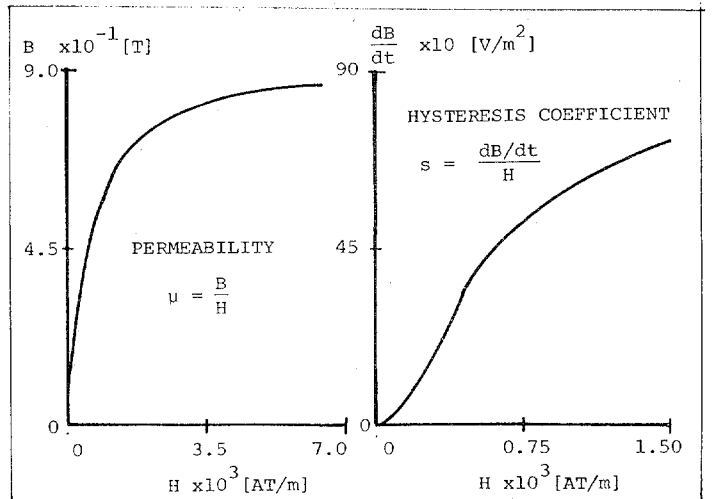


Fig. 4. Magnetization curves used in the calculations.

coils A,B,C,D. In order to show the effect of leakage fluxes from the iron core, each of the secondary coils was used as a secondary coil while the other secondary coils were opened.

Table 1. VARIOUS CONSTANTS USED IN THE CALCULATIONS.

Number of subdivisions in radial direction	6
Number of subdivisions in tangential direction	8
Limit of discrepancy	0.1 [percent]
Inner radius of iron core	0.04 [m]
Outer radius of iron core	0.05 [m]
Thickness of iron core	0.011 [m]
Thickness of primary coil	0.002 [m]
Thickness of secondary coil	0.002 [m]
Number of turns of primary coil	400 [turns]
Number of turns of secondary coil	200 [turns]
Space factor of iron	90 [percent]
Electric resistance of primary coil	5.57 [Ω]
Load resistance	102.3 [Ω]
Steady state	102.3 [Ω]
Transient state	3.3 [Ω]

All the initial fluxes are set to zero.

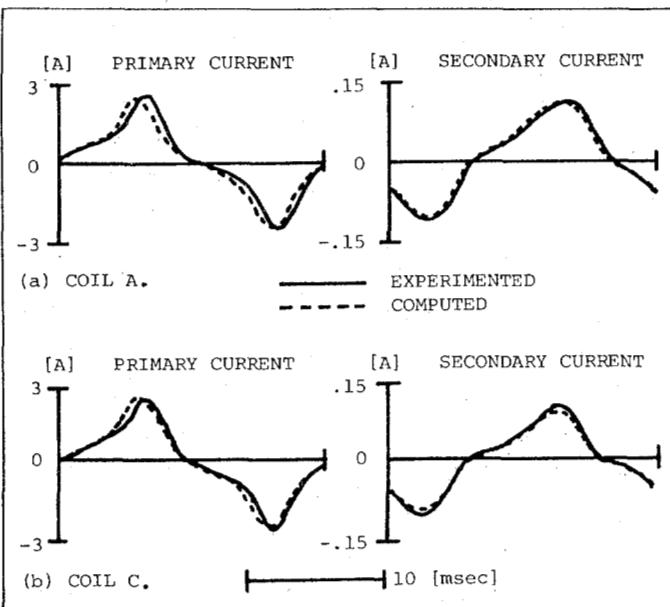


Fig. 5. Steady state primary and secondary currents when the impressed voltage is  $e_1 = \sqrt{2} \cdot 20 \cdot \sin(100\pi t)$ .

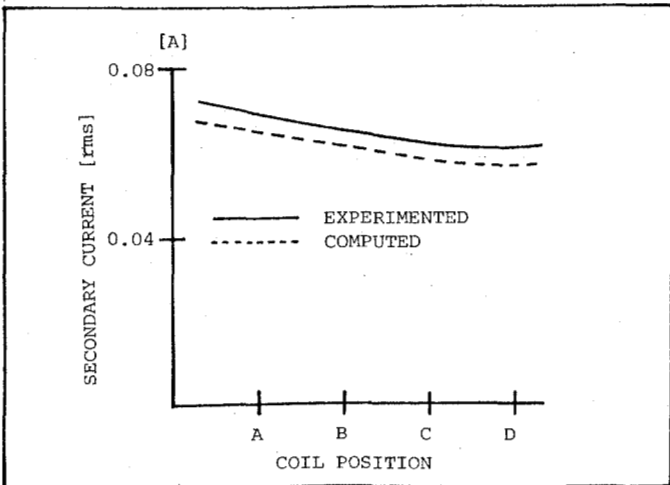


Fig. 6. Steady state secondary current difference in coil positions when the impressed voltage is  $e_1 = \sqrt{2} \cdot 20 \cdot \sin(100\pi t)$  and the currents are expressed in root mean square value.

Figure 5(a) shows the steady state primary and secondary currents when the coil A is used as a secondary coil. Also, Fig. 5(b) shows the steady state primary and secondary currents when the coil C is used as a secondary coil. Figure 6 shows the root mean square values of secondary current.

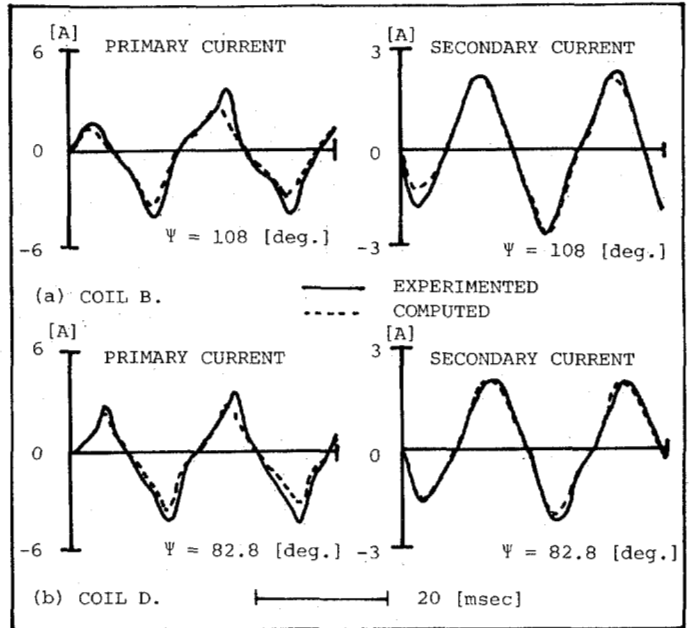


Fig. 7. Transient state primary and secondary currents when the impressed voltage is  $e_1 = \sqrt{2} \cdot 20 \cdot \sin(100\pi t + \psi)$ .

Figure 7(a) shows the transient state primary and secondary currents when the coil B is used as a secondary coil. Moreover, Fig. 7(b) shows the transient state primary and secondary currents when the coil D is used as a secondary coil.

CONCLUSION

As shown in Figs. 5-7, our model has behaved just like a practical toroidal transformer and given the 3-D solutions as accurate as 1-D solutions<sup>1,2</sup>. Consequently, it has been shown that the possibility of computerized design for transformers becomes much greater.

The time required to obtain the results of Fig. 7(a) was a few minutes on the computer ACOS-6/SYSTEM-700 at the Computer Center of Hosei University.

REFERENCES

- [1] Y. Saito, "Three-Dimensional Analysis of Magnetodynamic Fields in Electromagnetic Devices taken into account the Dynamic Hysteresis Loops," *IEEE Transaction on Magnetics*, Vol. MAG-18, No. 2, March 1982, pp. 546-551.
- [2] Y. Saito, H. Saotome and T. Yamamura, "A Lumped Circuit Model for Nonlinear Inductor exhibiting Dynamic Hysteresis Loops and Its Application to the Electric Circuits," *Comp. Meths. Appl. Mech. Eng.*, to be published.
- [3] Y. Saito, "Three-Dimensional Analysis of Nonlinear Magnetostatic Fields in a Saturable Reactor," *Comp. Meths. Appl. Mech. Eng.*, Vol. 16, No. 1, Oct. 1978, pp. 101-115.
- [4] Y. Saito, "Three-Dimensional Analysis of Nonlinear Magnetodynamic Fields in a Saturable Reactor," *Comp. Meths. Appl. Mech. Eng.*, Vol. 22, No. 3, June 1980, pp. 289-308.